Pramana – J. Phys. (2019) 93:48
https://doi.org/10.1007/s12043-019-1810-7

Excitation performance of $Ba_{0.8}Mg_{0.2}(Zr_{0.1}Ti_{0.8}Ce_{0.1})O_3$ materials in an electrical field

SUGATO HAJRA[1], MANISHA SAHU[1,*], BASANTA K PANIGRAHI[2] and R N P CHOUDHARY[3]

[1]Department of Electronics and Instrumentation, Siksha 'O' Anusandhan University, Bhubaneswar 751 030, India
[2]Department of Electrical Engineering, Siksha 'O' Anusandhan University, Bhubaneswar 751 030, India
[3]Department of Physics, Siksha 'O' Anusandhan University, Bhubaneswar 751 030, India
*Corresponding author. E-mail: manishafl@outlook.com

MS received 2 February 2019; revised 13 March 2019; accepted 25 March 2019; published online 10 July 2019

Abstract. Dense and stoichiometric $Ba_{0.8}Mg_{0.2}(Zr_{0.1}Ti_{0.8}Ce_{0.1})O_3$ (BMZTCO) ceramics have been synthesised and their excitation was experimentally evaluated by applying an electric field. The processed sample exhibits superior frequency-independent and temperature-dependent dielectric parameters. The prepared sample has combined the tetragonal and cubic phases of $BaTiO_3$ and Ce_2O_3. The Bode plots suggest non-Debye type of relaxation mechanism and positive temperature coefficient-type behaviour. The excitation intensity reaches a peak when the driving frequency matches with the natural frequency of the prepared sample.

Keywords. X-ray diffraction; impedance; dielectric; device performance.

PACS Nos 73.90.+f; 68.55.Jk; 07.05.Fb

1. Introduction

Lead (Pb)-based functional materials are of great interest due to their enhanced physical properties and are used mostly to develop ultrasonic detectors, capacitors, energy harvesting circuits, humidity sensors etc. [1–5]. These materials are promising entrants but many problems arise, in relation to their dumping and recycling as the fabrication and machine wastes of lead-based materials cause much pollution. Nowadays, several research teams are seriously investigating the fabrication of non-lead compounds because Pb-based materials are hazardous to both environment and human health [6]. Therefore, the development of lead-free electroceramics which are eco-friendly with humidity-sensitive electrical properties comparable to those of Pb-based ones is the need of the hour.

Among the many lead-free materials, $BaTiO_3$ (BT) is a promising entrant bearing a ABO_3 (perovskite) structure suitable for developing electronics and multilayer ceramic capacitors (MLCC) [7]. To enhance the physical properties of the BT pervoskite, various methods such as site engineering or ion doping are employed at various sites (A- or B-site). The grain growth is inhibited and the phase transition is suppressed in BT modified with Ce^{4+} [8]. The phase transition temperature is strongly influenced by the doping of Zr in BT (Curie temperature shifts towards lower temperatures) [9]. The microstructure-related electrical properties are enhanced in the Mg-doped BT [10].

In this context, this work aims at understanding the evolution of phase, surface morphology and the analysis of dielectric parameters, including impedance, which have been systematically studied. The relaxation mechanism is realised using complex impedance spectroscopy. To realise the influence of the applied field, the BMZTCO component is placed between the electrodes forming a parallel plate capacitor arrangement. The receptivity of the electric field fortifies the BMZTCO component as a base for device engineering.

2. Sample processing and experimental techniques

The BMZTCO ceramic has been fabricated by a high-temperature ceramic preparation route using barium carbonate ($BaCO_3$) (CDH limited; 99%), titanium dioxide (TiO_2) (Loba Chemie; 99.5%), magnesium oxide (MgO) (Merck; 95%), zirconium dioxide (ZrO_2) (Himedia; 99%) and cerium (IV) oxide (CeO_2) (Loba Chemie; 99.95%) as per requirement. The wet (methanol) and dry mixing of ingredients were

mechanically ground using a mortar and pestle. Calcination was carried out at 1100°C for 4 h, and the calcined powder was examined using a powder diffractometer (Rigaku Ultima IV) using Cu Kα radiation ($\lambda = 1.54051$ Å; 2θ range of $20° \leq \theta \leq 80°$) with a 3°/min scanning speed. The green pellets (diameter = 12 mm and thickness = 1.5–2 mm) were compacted by blending of polyvinyl alcohol and a uniaxial isostatic pressure of 25 MPa. The pellets were sintered at 1120°C for 4 h, and one of the pellets was painted using high-purity silver paint which acts as an electrode for carrying out the electrical measurements. The computer-controlled impedance meter (N4L, UK) was employed for the dielectric and impedance analysis over a temperature range ($25 - 500$°C) and frequency ranging from 1 kHz to 1 MHz. Field emission scanning electron microscopy (FE-SEM; Quanta 200 FEG, The Netherlands) was used to check the morphology of the natural surface of the sintered pellet. The experimental set-up diagram for the excitation of the component is provided as the inset in figure 5 where the function generator and digital signal oscilloscope are from Aplab, India.

3. Results and analysis

Figure 1a represents the X-ray diffraction (XRD) pattern of the calcined BMZTCO powder. In this pattern, the black line corresponds to the experimental diffraction data at room temperature of the sample. The pattern and phase analysis of the material are similar to those of the reported one [11]. The experimental data are found to be matched with the previous reference pattern of $BaTiO_3$ (illustrated by a red stick), and CeO_2 (illustrated by a blue stick) bearing JCPDS Card Nos 01-074-1960 [12] and 00-043-1002 [13], respectively, with some unknown impurity. The crystallographic information of $BaTiO_3$ is $a = b = 3.988$ Å, $c = 4.0120$ Å, $\alpha = \beta = \gamma = 90°$ with tetragonal symmetry while CeO_2 has $a = b = c = 5.4113$ Å, $\alpha = \beta = \gamma = 90°$ with cubic symmetry. Figure 1b shows the micrograph and morphology of the prepared sample, imaged by an electron microscope in the scanning mode at 25°C (RT). High densification of the compacted ceramic samples is observed in the microstructures. The bulk density of the pressed pellet is 7.04 g/cm^3 and the theoretical density is 8.00 g/cm^3. The XRD data were used to determine the sample density by comparing the theoretical density with the measured bulk density of the sample pellet obtained after sintering. The micrograph shows the homogeneous distribution of grains of different sizes with a certain degree of porosity, suggesting the formation of good-quality ceramic samples.

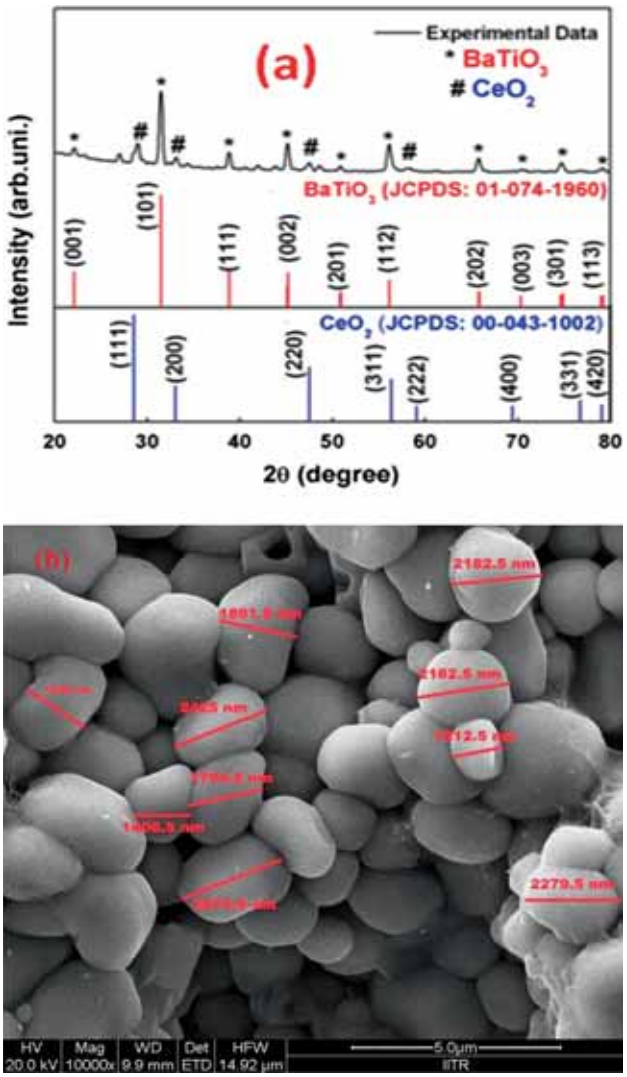

Figure 1. (**a**) XRD spectrum at room temperature and (**b**) surface micrograph of the natural surface of BMZTCO.

Figures 2a and 2b present the temperature-dependent dielectric parameters (permittivity and loss) at the selected frequency. The ferroelectric phase transition temperature moves ahead of the experimental temperature limit. This may be due to the space-charge polarisation or diffusion of ions taking place with an increment in temperature [14]. Additionally, thermal energy leads to cross the activation barrier for the orientation of polar molecules in the direction of the field which increases the permittivity value [15]. The normal ferroelectric material shows no shift in the dielectric peak with increasing frequency. In the case of the relaxor material, there is a shift in transition temperature or the shifting of a broadened peak towards higher temperature [16]. It exhibits the temperature-dependent tangent loss ($\tan\delta$). Similar to the relative dielectric constant, $\tan\delta$ increases slowly with the rising temperature.

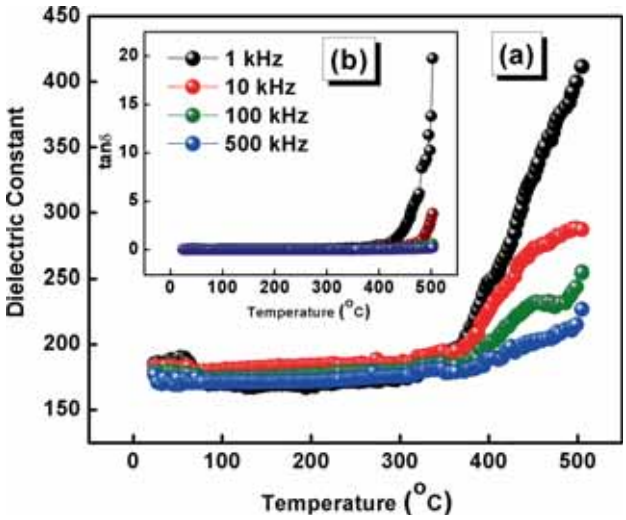

Figure 2. Temperature-dependent (**a**) dielectric constant and (**b**, inset) loss factor of BMZTCO at selected frequencies.

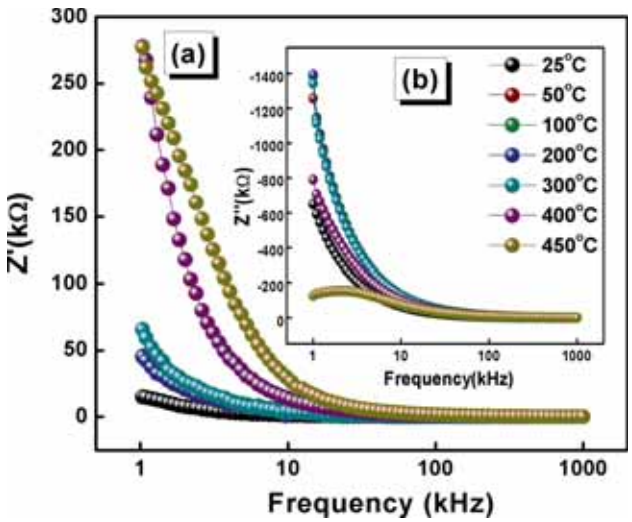

Figure 3. Frequency-dependent (**a**) real part and (**b**, inset) imaginary part of impedance of BMZTCO at selected temperatures.

But it increases sharply beyond 400°C because of the scattering of charge carriers and defects created at higher temperatures in the material [17]. In addition to this, the ferroelectric domain wall energy makes less contribution to the loss factor at higher temperatures, and as a result, the value of tan δ enhances [18].

The capacitive and the resistive properties of the materials are vital to the device applications of the dielectric materials. Impedance spectroscopy is a vital technique to study the dynamics of mobile and bound charges in the bulk and interfacial areas of the prepared sample [19]. The real (Z') and the imaginary (Z'') components of complex impedance ($Z = Z' - jZ''$) can be expressed as: $Z' = R/[1 + (\omega\tau)^2]$ and $Z'' = \omega R\tau/[1 + (\omega\tau)^2]$ [20], where symbols have the usual meaning. Figure 3a clearly illustrates that at low-frequency range, Z' has a higher value, and it enhances with the increment in the temperature. This shows positive temperature coefficient resistance behaviour (PTCR) as the magnitude of Z' increases with the rise in temperature. In the region of high frequency, Z' becomes frequency-independent, irrespective of the temperature difference, indicating the reluctance/inertia of the space charge in following the fast varying electric field. The frequency dependence of Z'' is presented in the inset of figure 3b. It shows the appearance of a characteristic frequency. This characteristic frequency is observed to increase with the increment in temperature, suggesting that the relaxation process is dependent on temperature. It is depicted that at room temperature, the peaks are prominent, and at high temperature, it broadens. This suggests the sharing of relaxation time with temperature. The immobile species contribute to the low temperature, and at high temperature, the activation of defects

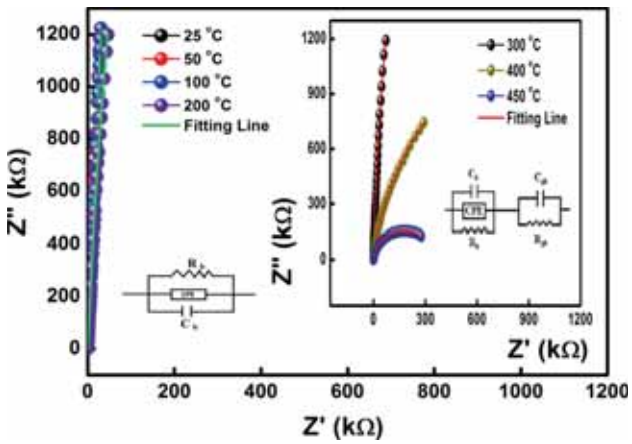

Figure 4. Z' vs. Z'' (Nyquist plot) of BMZTCO samples at different temperatures.

contributes towards the relaxation process [21,22]. Figure 4 and the inset illustrate the Nyquist plot which represents Z' vs. Z'' at different temperatures. Successive semicircles are formed in this plot in which the first circle (higher frequency) represents the grain/bulk effect, the second circle (intermediate frequency) represents the grain boundary effect and the third circle (lower frequency) represents the electrode effect [23]. It is clearly seen from the plot that there is a deviation from the ideal Debye-type behaviour which may be due to grain inhomogeneity. The suitable circuit model is shown in figure 4 and the inset. The computer software Zsimpwin helps to fit experimental impedance data to an equivalent electrical circuit. The single semicircular arcs are well fitted with equivalent circuits (as

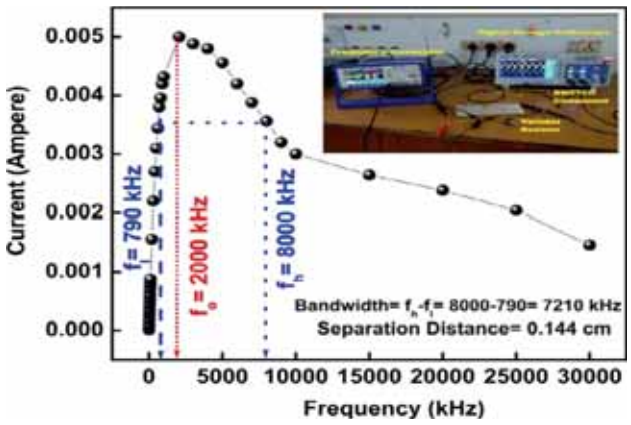

Figure 5. Frequency characteristics across the surface of the BMZTCO component and (inset) experimental set-up to drive the component through an electric field induced by a parallel plate capacitor.

shown in figure 4) made up of resistance (R), capacitance (C) and constant phase element (Q) for 25, 50, 100 and 200°C while the data that exhibit two semicircles are represented by an equivalent network made up of RQC and RC circuits connected in series (shown in figure 4 (inset)) for 300, 400 and 450°C. The two semicircles correspond to the grain and grain boundary effect.

The excitation of the prepared sample through the applied electric field was investigated by an experimental set-up (inset in figure 5). The set-up design mainly comprises a frequency generator, digital signal oscilloscope, variable resistor, and a parallel plate capacitor. The voltage across the component caused by excitation is measured by soldering two lead wires on the silver surface electrodes of the prepared component. The component is polarised when implanted in an applied electric field. Consequently, across the component surface, a voltage is seen. If the electric field frequency matches the natural frequency of the component, an electrical resonance can be excited. During resonance, the reactive component of the structure becomes zero, and so the system acts purely resistive. As the system is resistive, the magnitude of the current is high leading to a large voltage across the surface of the sample. Before resonance, the structure is capacitive in nature, and after resonance, the structure is inductive. Figure 5 shows the frequency-dependent current across the sample. It is depicted that the component gets excited as the parallel plate capacitor generates the field responsible for the polarisation of the component and at 2000 kHz, maximum current (I_{max}) was obtained when the operating frequency is matched with the natural resonance frequency of the sample. This result affirms the influence of electric field on the fabricated component.

4. Conclusion

The ceramic sample of BMZTCO was prepared by a standard mixed oxide reaction at high temperature. Preliminary structural studies suggest that BMZTCO has $BaTiO_3$ and CeO_2 phases with a few unknown impurities. High densification of grains on the natural surface of the ceramic sample was observed using FE-SEM studies. The temperature-dependent dielectric parameters (loss and permittivity) follow a similar trend. It rises with increment with temperature for the selected frequencies. The Nyquist plot shows the contribution of both grain and grain boundaries. The PTCR behaviour of the sample is affirmed from the impedance analysis. The excitation of the component was examined practically by applying external electric field through a parallel plate capacitor. The fabricated material acts as a promising entrant to be used in the preparation of passive electronic components.

Acknowledgement

SH and RNPC would like to sincerely thank Prof. K L Yadav, Department of Physics, IIT Roorkee for his assistance with surface micrograph imaging in his laboratory.

References

[1] H Yang, P Liu, F Yan, Y Lin and T Wang, *J. Alloys Compd.* **773**, 244 (2019)
[2] X Liu, H Yang, F Yan, Y Qin, Y Lin and T Wang, *J. Alloys Compd.* **778**, 97 (2019)
[3] H Yang, F Yan, Y Lin, T Wang, F Wang, Y Wang, L Guo, W Tai and H Wei, *J. Eur. Ceram. Soc.* **37**, 3303 (2017)
[4] H Yang, F Yan, Y Lin and T Wang, *ACS Sustain. Chem. Eng.* **5**, 10215 (2017)
[5] F Yan, H Yang, L Ying and T Wang, *J. Mater. Chem. C* **6**, 7905 (2018)
[6] M De and H S Tewari, *Pramana – J. Phys.* **89**: 3 (2017)
[7] V S Puli, D K Pradhan, D B Chrisey, M Tomozawa, G L Sharma, J F Scott and R S Katiyar, *J. Mater. Sci.* **48**, 1 (2012)
[8] J H Hwang and Y H Han, *J. Am. Ceram. Soc.* **84**, 1750 (2001)
[9] R Kumar, K Asokan, S Patnaik and B Birajdar, *AIP Conf. Proc.* **1731**, 030025 (2016)
[10] W Cai, C L Fu, J C Gao and C X Zhao, *Adv. Appl. Ceram.* **110**, 181 (2011)
[11] W Mao, W Chen, X Wang, Y Zhu, Y Maa, H Xue, L Chu, J Yang, X Li and W Huang, *Ceram. Int.* **42**, 12838 (2016)
[12] S Miyake and R Ueda, *J. Phys. Soc. Jpn.* **2**, 93 (1947)

[13] D Geier and G McCarthy, *ICDD grant in aid* (North Dakota State University, North Dakota, USA, 1991)
[14] J M Sailaja, N Murali, S J Margarette, T W Mammo and V Veeraiah, *Results Phys.* **8**, 128 (2018)
[15] K V Babu, L Seeta Devi, V Veeraiah and K Anand, *J. Asian Ceram. Soc.* **4**, 269 (2016)
[16] F Moura, A Z Simoes, B D Stojanovic, M A Zaghete, E Longo and J A Varela, *J. Alloys Compd.* **462**, 129 (2008)
[17] M Sahu, S K Pradhan, S Hajra, B K Panigrahi and R N P Choudhary, *Appl. Phys. A* **125**, 183 (2019)
[18] D Pal and J L Pandey, *Bull. Mater. Sci.* **33**, 691 (2010)
[19] H Yang, F Yan, G Zhang, Y Lin and F Wang, *J. Alloys Compd.* **720**, 116 (2017)
[20] M Sahu, S Hajra and R N P Choudhary, *SN Appl. Sci.* **1**, 13 (2019)
[21] B K Singh and B Kumar, *Cryst. Res. Technol.* **45**, 1003 (2010)
[22] P Kumari, R Rai, S Sharma and M A Valente, *J. Adv. Dielectr.* **7**, 1750034 (2017)
[23] K Parida, S K Dehury and R N P Choudhary, *Mater. Sci. Eng. B* **225**, 173 (2017)